Supporting Information

Redox properties of plant biomass-derived char black carbon (biochar)

Laura Klüpfel[†], Marco Keiluweit[§,‡], Markus Kleber[§,¶], and Michael Sander[†,*]

[†] Department of Environmental Systems Sciences
Institute of Biogeochemistry and Pollutant Dynamics
Swiss Federal Institute of Technology (ETH) Zurich, 8092 Zurich, Switzerland

§ Department of Crop and Soil Science
Soil and Environmental Geochemistry
Oregon State University, Corvallis, OR 97331, United States
¶ Institute of Soil Landscape Research, Leibniz-Center for Agricultural Landscape Research (ZALF), 15374 Müncheberg, Germany

[‡] Department of Environmental Earth System Science
Soil and Environmental Biogeochemistry
Stanford University, Stanford, CA 94305, USA

Submitted to
Environmental Science & Technology

*To whom correspondence should be addressed.
E-mail: michael.sander@env.ethz.ch
Phone: +41-(0)44 6328314
Fax: +41 (0)44 633 1122

Number of pages: 22
Number of figures: 9
Number of tables: 7
Number of words: 5622

Physicochemical properties of analyzed char specimens. **Table S1** provides an overview of selected physicochemical properties of the tested chars.

Table S1. Selected physicochemical properties of the 19 analyzed char specimen. The properties include char elemental composition, C/H ratio, double bond equivalents (DBE), aromaticity index (AI), and spectroscopic quinoid C=O contents.

Char	Feedstock	Elemental composition [mmol element (g char)$^{-1}$][a]				C/H ratio[b]	C/O ratio[b]	DBE[c] per C [mol DBE (mol C)$^{-1}$]	AI[c] [mol DBE_{AI} (mol C_{AI})$^{-1}$]	Quinoid C=O[d] content [mmol C=O (g char)$^{-1}$]	Quinoid C=O content ([O])$^{-1}$ [%]
		C	N	H	O	[mol_C/mol_H]	[mol_C/mol_O]				
G700	grass	78.4	0.50	15.3	2.3	5.2	34.9	0.92	0.92	0.80	35.4
G600		74.1	0.71	24.7	4.8	3.0	15.6	0.85	0.85	1.66	35.0
G500		68.4	0.78	33.2	8.4	2.1	8.2	0.78	0.75	2.60	31.0
G400		64.4	0.89	47.0	10.4	1.4	6.2	0.66	0.60	2.79	26.7
G300		49.7	0.73	66.4	20.4	0.8	2.4	0.36	0.00	2.33	11.4
G200		39.3	0.44	71.1	28.2	0.6	1.4	0.13	0.00	0.25	0.9
W700	wood	76.8	0.06	16.1	3.8	4.8	20.5	0.91	0.90	1.2	33.3
W600		74.1	0.04	29.7	5.0	2.5	14.8	0.81	0.80	1.7	34.3
W500		68.2	0.06	35.1	9.1	1.9	7.5	0.76	0.72	2.8	31.0
W400		61.7	0.04	49.1	13.1	1.3	4.7	0.62	0.52	3.1	23.9
W300		45.6	0.04	64.5	24.2	0.7	1.9	0.32	0.00	1.7	7.0
W200		42.4	0.03	68.9	26.4	0.6	1.6	0.21	0.00	-	-
HZ700	hazelnut										
HZ550											
HZ400											
DF700	douglas fir										
DF400											
RS450	rice straw	58.1	0.57	10.9	7.3	5.29	8.0	0.93	0.92	1.5	20.3
CW450	chestnut wood	79.2	0.36	10.9	2.1	7.20	38.4	0.95	0.95	0.5	23.7

[a.] Elemental composition data from reference[1] [b.] Calculated from elemental composition data. [c.] Calculation of the aromaticity index (AI) and double binding equivalents (DBE) according to reference.[2] The calculation is detailed in the last section of this Supporting Information [d.] Quinoid C=O contents based on NEXAFS spectra from reference [1] (the calculations are described in detail below).

Particle size distributions of chars. All chars were finely ground in Eppendorf tubes using ball mills (Retsch MM200 and MM301; 750 min^{-1}; 10 min). Prior to milling, three large (Ø 2.8 mm) and five small (Ø 1.4 mm) zirconium oxide balls were added to each tube. The resulting particle size distributions of the ground chars were determined by laser diffraction (Beckman Coulter, LS 13 320). Prior to the measurement, the char suspensions (1 g L^{-1}) were positioned in a water bath underneath an ultrasonic tip (Sonics Vibra-cell VCX 500 with microtip, amplitude 150 W, 10 min) to finely disperse the chars. Aliquots of 2-5 mL of the dispersed char suspensions were injected into a sampling module (universal liquid module, 120 mL deionized water) until an obscurity of 8-11% was reached. Subsequently, triplicate measurements of 60 sec each were taken. The three measurements were averaged to obtain the final particle size distribution. The cumulative particle size distributions are given in **Figure S1**.

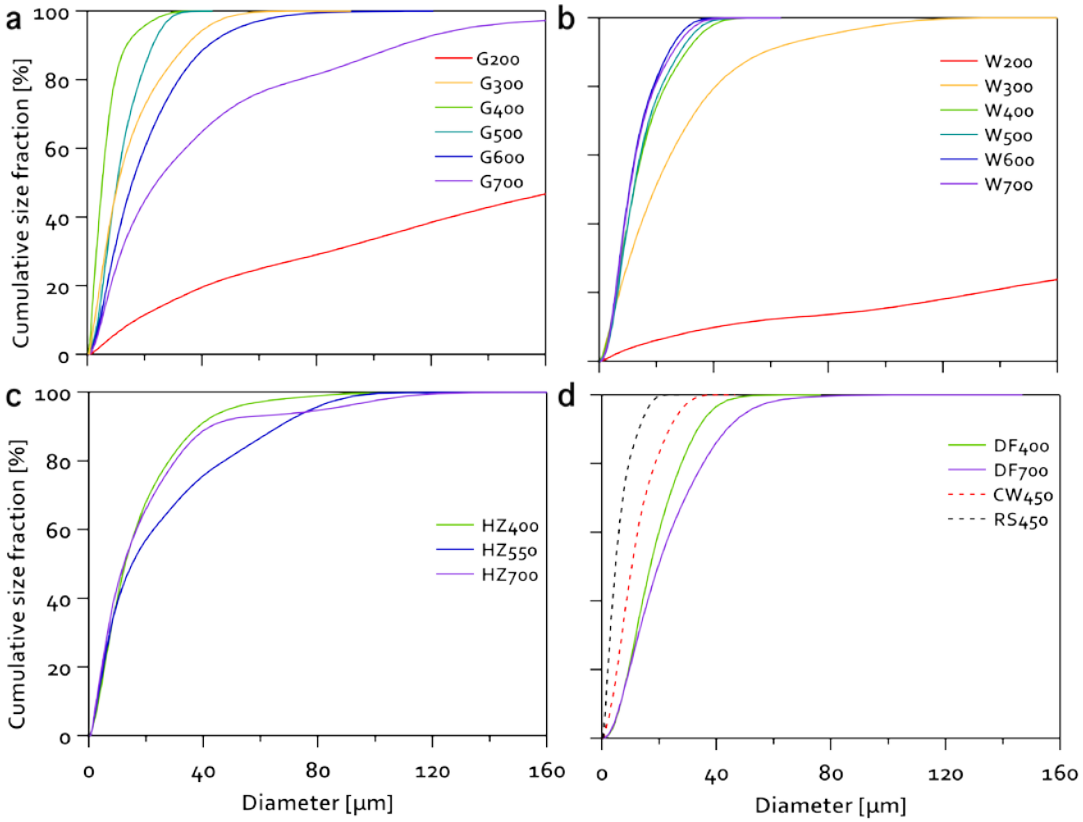

Figure S1. Cumulative particle size distributions of grass (G; panel a), wood (W; panel b), and hazelnut (HZ; panel C) thermosequence chars. Panel d shows the cumulative particle size distributions of douglas fir (DF), chestnut wood (CW) and rice straw (RS) chars.

Electron accepting and donating capacity (EAC and EDC) values. The EAC and EDC values reported in the manuscript were calculated by normalizing the number of transferred electrons to total char masses (i.e., the reported EAC and EDC values have units of [mmol e^- (g char)$^{-1}$]). Because the electrochemical data and the low contents of Mn and Fe in the chars (data in **Table S5**) strongly suggest that organic moieties/entities dominated the redox properties of the tested chars (as detailed below), we assessed whether the trends in EAC and EDC with HTTs reported in the manuscript were different when normalizing the number of transferred electrons to ash-content corrected char masses or to elemental carbon contents. The ash contents of the chars are provided in **Table S2**.

Table S2. Ash contents of the thermosequence char specimen determined by gravimetric analysis. The data is taken from reference[1], which also provides experimental details on how these contents were obtained.

Heat treatment temperature (HTT)	Ash contents [%]	
[°C]	Grass chars	Wood chars
700	19.3	1.7
600	18.9	3.7
500	15.4	2.1
400	16.3	1.4
300	9.4	1.5
200	5.7	1.5

Figure S2 shows that the different normalizations resulted in similar trends of the EAC and EDC values with HTT.

The normalization of transferred electrons to total char mass has the advantage that the analyzed char masses were known for all chars and hence that the EAC and EDC values of the different chars could be compared. A comparison would not have been possible with the other two normalization procedures as the elemental compositions and ash-contents were available only for the wood and grass thermosequence chars.

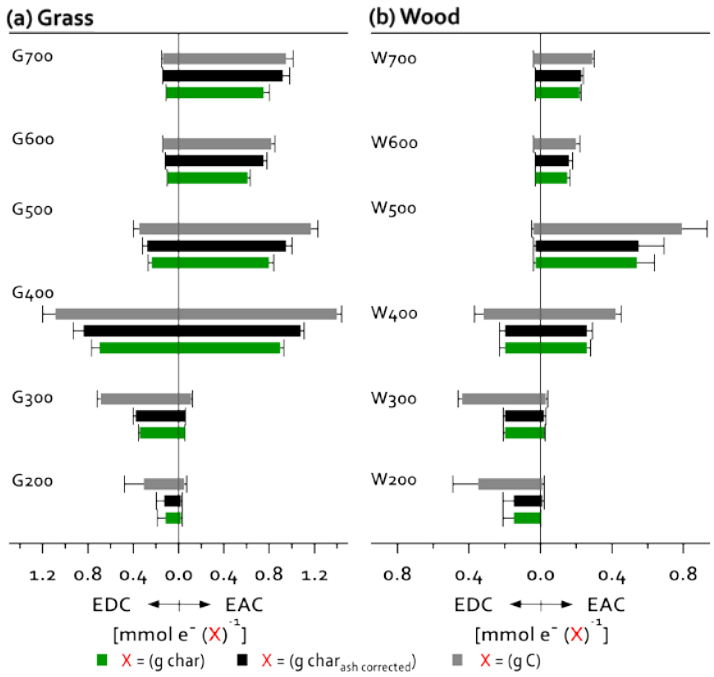

Figure S2. Electron donating capacities (EDC) and electron accepting capacities (EAC) reported on the basis of total char mass (i.e., units of [mmol e^- (g char)$^{-1}$]) (green bars), char mass corrected for ash contents (i.e., units of [mmol e^- (g $char_{ash\ corrected}$)$^{-1}$] (black bars), and total carbon contents of the chars (i.e., units of [mmol e- (g C)$^{-1}$] (grey bars). The relative trends in EAC and EDC values with heat treatment temperature (HTT) are the same for all three normalizations.

The inorganic ash-fraction of the grass and wood thermosequence chars was analyzed for the presence of crystalline mineral phases using X-ray diffraction (XRD). The respective XRD scans are published elsewhere[1]. XRD was unable to detect crystalline mineral phases in wood chars but indicated the presence of redox-inactive Sylvite [KCl], Calcite/Aragonite [$CaCO_3$], Dolomite [$CaMg(CO_3)_2$], and Quartz [SiO_2] as well as traces of other phases in grass chars. Peak intensities of mineral phases varied as a function of HTT, with signal intensities of carbonates growing stronger in high HTT chars.

Ubiquinone addition experiment. To assess the extents to which MER detects reducible (quinone) moieties on the surfaces of the analyzed chars, we pre-adsorbed increasing concentrations of an exogenous quinone to selected chars and subsequently analyzed these chars

by MER. We chose the highly apolar ubiquinone, Q_{10}, as exogenous quinone because it strongly adsorbed to the char surfaces.

Adsorption experiment. Increasing amounts of Q_{10} were added from an ethanolic stock solution ($c(Q_{10})$= 0.94 ± 0.01 mM; determined by MER) to suspensions of G500 and G400 chars (both at 1 g L^{-1}) to final adsorbed Q_{10} concentrations between 0.19 and 0.53 mmol Q_{10} (g G500)$^{-1}$ and between 0.19 and 0.76 mmol Q_{10} (g G400)$^{-1}$. The char suspensions were stirred for 30 min to allow for attainment of Q_{10} adsorption equilibrium. The EAC and EDC values chars were subsequently determined using MER and MEO.

Q_{10} adsorption to chars. The extents of Q_{10} adsorption to the chars were determined as follows: After the addition of Q_{10} to the char suspensions and adsorptive equilibration, aliquots (0.5 mL) of the suspensions of both Q_{10}-free control chars (only chars, no Q_{10} added) and the Q_{10}-amended chars were centrifuged (at 9000 rpm, 5 min). The supernatants of the centrifuged char samples were then analyzed using MER and MEO. Analysis of the supernatants of the Q_{10}-free chars did not show reductive and oxidative current responses in MER and MEO, respectively, confirming that the current responses measured for the char suspensions resulted from electron transfer to/from the suspended char particles. The supernatants of Q_{10}-amended chars showed small reductive current signals in MER. **Table S3** shows the nominal dissolved concentrations of Q_{10} in each amended char sample (assuming that all of the added Q_{10} remained dissolved) and, following centrifugation, the averages and ranges of duplicate EAC measurements of the corresponding supernatants. These EAC values were obtained from integration of the reductive current responses in MER. The EAC values of the supernatants were always much smaller than the theoretical number of electrons transferred to the supernatants if all Q10 had remained dissolved. The analysis showed that only between approximately 3 to 8 % of the added Q_{10} remained dissolved whereas the major fractions of the added Q_{10} adsorbed the char surfaces.

Table S3. Extent of adsorption of added ubiquinone, Q_{10}, to the G500 and G400 chars. Given are the nominal dissolved concentrations of Q_{10}, $c(Q_{10})$, in each char suspension and the measured EAC values of the supernatant of each sample following centrifugation. The last column compares the number of electrons transferred to the supernatants to the theoretical number of electrons that would have been transferred if all added Q_{10} had remained in solution.

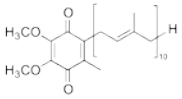	$c(Q_{10,\ total})$ [mmol Q_{10} $(L)^{-1}$]	$EAC_{supernatant}$ (± range) [mmol e^- $(L)^{-1}$]	$EAC_{supernatant}$ $(2 \times c(Q_{10,\ total}))^{-1}$ (± range) [%]
G500	0.16	n.d.	n.d.
	0.22	n.d.	n.d.
	0.31	0.04 ± 0.015	6.5 ± 2.4
	0.42	0.03 ± 0.005	3.6 ± 0.6
G400	0.16	0.02 ± 0.008	6.3 ± 2.5
	0.22	0.03 ± 0.007	6.8 ± 0.3
	0.31	0.05 ± 0.013	8.1 ± 0.8
	0.42	0.07 ± 0.078	8.3 ± 9.3

Expected EAC values of Q_{10}-amended char samples. We calculated the expected EAC values of the char specimens amended with Q_{10} (i.e., $EAC_{expected}$ [mmol e- (g char)$^{-1}$]) according to:

$$EAC_{expected} = EAC_{char} + \frac{2 \times n_{Q10}}{m_{char}} \qquad \textbf{Eq. S1}$$

where EAC_{char} [mmol e- (g char)$^{-1}$] is the EAC of the untreated char (i.e., no pre-adsorbed Q_{10}), n_{Q10} [mmol Q_{10}] is the number of Q_{10} molecules added, and m_{char} [g] is the mass of the char to which Q_{10} was adsorbed. n_{Q10} is multiplied by a factor of 2 [mmol e- (mmol Q_{10})$^{-1}$] to account for the fact that each Q_{10} molecule accepts two electrons. The expected EAC values are compared to the measured EAC values of the char suspensions in **Figures 1e** (G400) and **1f** (G500) in the manuscript.

Effects of charring conditions on char redox properties. To assess pyrolysis effects other than HTT on the redox properties of chars, we quantified the EAC and EDC values of an additional six chars formed at HTT of 400/450° C and 700°C and from different feedstock. The results are shown in **Figure S3.**

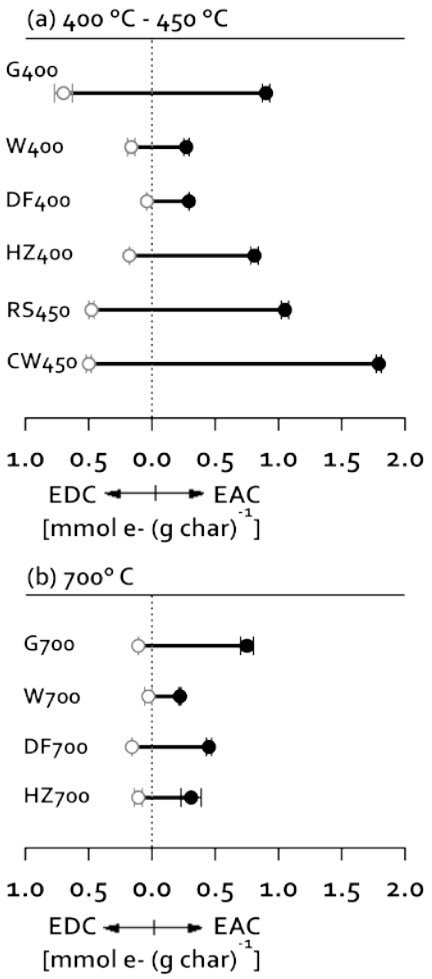

Figure S3. Electron accepting capacities (EACs) (closed symbols), electron donating capacities (EDCs) (open symbols) and the corresponding electron exchange capacities (EECs) (horizontal black bars) of chars formed at (a) 400° C and 450°C and (b) 700° C from different feedstock (i.e., grass (G), wood (W), douglas fir (DF), hazelnut (HZ), rice straw (RS), and chestnut wood (CW)). The data for G400, G700, W400, and W700 are re-plotted from Figure 2.

Redox cycling of chars. To assess the reversibility of the electron transfer to/from the chars, we quantified the redox states of all chars prior to chemical reduction (i.e., untreated chars), following chemical reduction by $NaBH_4$ (i.e., reduced chars), and following O_2 re-oxidation (i.e., re-oxidized chars). *Char reduction.* A five mL aliquot of each char suspension (4 g_{char} L^{-1}) was transferred inside the glovebox to a glass vial that contained 30 mg $NaBH_4$. In addition to reducing the chars, BH_4^- also reduced protons in solution, resulting in H_2 formation. The vials were therefore repeatedly vented. After 7 days, which was sufficiently long for the reaction to run to completion, the glass vial was purged with N_2 to remove formed H_2 gas from the solution. Proton reduction caused an increase of the pH to values between pH 8 and 9. The pH was re-adjusted to pH 7 inside the glovebox using anoxic, concentrated HCl. The reduced char samples were subsequently analyzed using MER and MEO. *Char re-oxidation.* Three mL aliquots of all reduced char suspensions were transferred to separate glass vials that were stoppered and transferred out of the glovebox. The headspace of all samples was exchanged through the stopper with air for 30 sec, followed by storing each vial on a horizontal shaker at 25°C in the dark. The exchange of the headspace with air was carried out a second and a third time, two and four days after the first exchange. After a total of seven days, each vial was purged with N_2 for 10 min to remove unreacted O_2. The vials were placed back onto the shaker for 17 h to allow for diffusion of remnant O_2 out of the chars. The N_2 purging was repeated for 5 min, followed by transfer of the vials back into the glovebox for MER and MEO analyses.

The EAC and EDC values and the corresponding EEC values of all chars are shown in **Table S4.** The relative contributions of EAC and EDC values to the EEC values of the native, reduced, and re-oxidized HZ, DF, RS and CW chars are shown in **Figure S4.** The respective data for the grass and wood thermosequence chars are shown in **Figure 3** in the manuscript.

Table S4. Electron accepting capacities (EACs), electron donating capacities (EDCs) and electron exchange capacities (EEC=EAC+EDC) of untreated (native), chemically reduced (with sodium borohydride), and re-oxidized (with O_2) char specimen. The EAC and EDC values were determined by mediated electrochemical reduction (MER; E_h=-0.49V, pH 7) and mediated electrochemical oxidation (MEO; E_h=+0.61V, pH 7), respectively, and are reported as averages ± standard deviation from triplicate analyses.

Char	Feedstock	Untreated			Reduced			Re-oxidized		
		EAC	EDC	EEC	EAC	EDC	EEC	EAC	EDC	EEC
		[mmol e^- (g char)$^{-1}$]			[mmol e^- (g char)$^{-1}$]			[mmol e^- (g char)$^{-1}$]		
G700	Grass	0.75±0.05	0.11±0.00	0.86±0.05	0.31±0.01	0.43±0.06	0.75±0.08	0.51±0.04	0.05±0.01	0.56±0.04
G600		0.61±0.02	0.10±0.00	0.71±0.02	0.21±0.01	0.32±0.06	0.52±0.06	0.53±0.01	0.06±0.02	0.59±0.02
G500		0.80±0.04	0.24±0.03	1.04±0.02	0.42±0.01	0.60±0.01	1.02±0.01	0.81±0.04	0.26±0.02	1.07±0.06
G400		0.90±0.03	0.70±0.07	1.60±0.08	0.27±0.00	1.59±0.04	1.86±0.05	0.45±0.02	0.76±0.03	1.21±0.02
G300		0.06±0.00	0.34±0.01	0.40±0.01	0.04±0.03	0.31±0.05	0.36±0.02	0.28±0.04	0.80±0.04	1.14±0.04
G200		0.02±0.01	0.12±0.07	0.14±0.07	0.01±0.00	0.37±0.17	0.38±0.17	0.02±0.00	0.24±0.12	0.26±0.12
W700	Wood	0.22±0.07	0.03±0.00	0.25±0.01	0.07±0.02	0.08±0.02	0.15±0.04	0.10±0.02	0.01±0.00	0.10±0.02
W600		0.15±0.01	0.03±0.00	0.18±0.02	0.00±0.00	0.07±0.01	0.07±0.01	0.04±0.01	0.02±0.00	0.06±0.01
W500		0.54±0.10	0.03±0.01	0.59±0.09	0.28±0.03	0.15±0.01	0.43±0.03	0.45±0.04	0.04±0.00	0.49±0.03
W400		0.26±0.02	0.20±0.03	0.46±0.04	0.12±0.01	0.59±0.03	0.71±0.04	0.22±0.01	0.48±0.03	0.70±0.04
W300		0.02±0.00	0.20±0.01	0.21±0.01	0.02±0.01	0.34±0.15	0.36±0.15	0.09±0.00	0.44±0.03	0.53±0.03
W200		0.005±0.00	0.15±0.06	0.15±0.06	0.00±0.00	0.21±0.07	0.21±0.07	0.03±0.00	0.24±0.04	0.26±0.04
HZ700	Hazelnut	0.31±0.08	0.11±0.03	0.42±0.10	0.08±0.04	0.12±0.01	0.20±0.05	0.13±0.00	0.02±0.00	0.15±0.00
HZ550		0.33±0.05	0.14±0.01	0.46±0.06	0.12±0.03	0.34±0.01	0.47±0.02	0.31±0.03	0.08±0.02	0.39±0.03
HZ400		0.81±0.03	0.18±0.00	0.98±0.03	0.36±0.01	0.56±0.06	0.92±0.07	0.78±0.05	0.24±0.01	1.03±0.07
DF700	Douglas fir	0.45±0.02	0.16±0.00	0.61±0.02	0.08±0.01	0.65±0.02	0.73±0.01	0.35±0.05	0.06±0.01	0.41±0.05
DF400		0.29±0.00	0.04±0.00	0.34±0.01	0.04±0.00	0.29±0.05	0.33±0.05	0.22±0.01	0.06±0.00	0.28±0.01
RS450	Rice straw	1.05±0.03	0.48±0.02	1.53±0.04	0.23±0.05	1.21±0.08	1.44±0.03	0.73±0.03	0.93±0.03	1.66±0.06
CW450	Chestnut wood	1.79±0.02	0.50±0.02	2.28±0.04	0.88±0.00	1.83±0.15	2.71±0.15	1.67±0.05	1.96±0.14	3.63±0.17

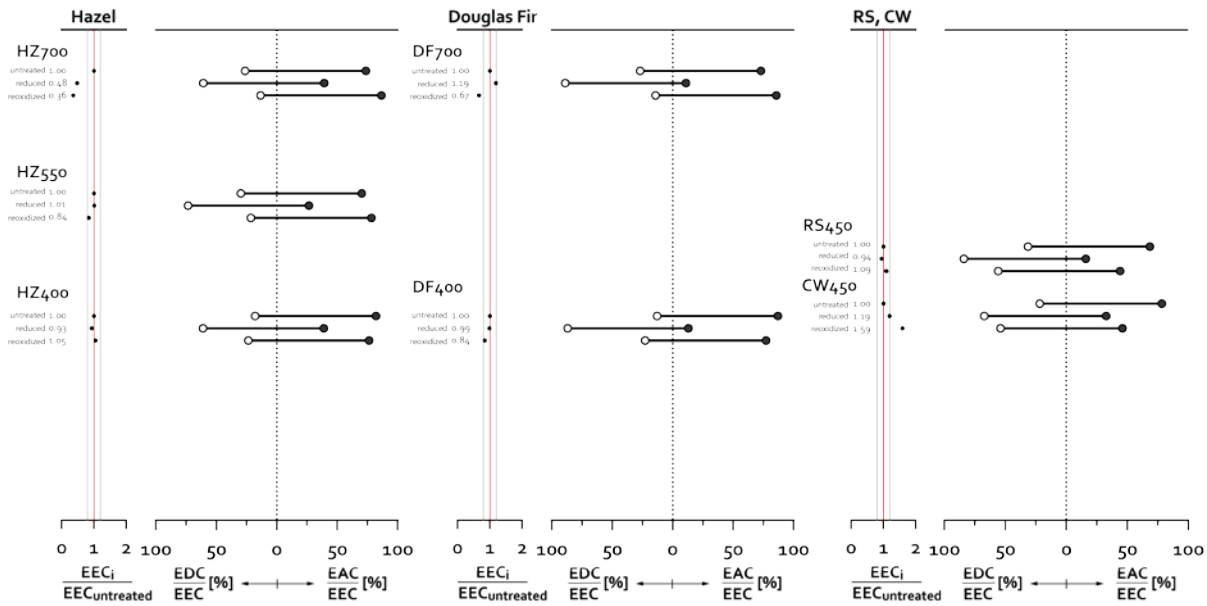

Figure S4. Changes in the electron accepting capacities (EACs) (black symbols), electron donating capacities (EDCs) (open symbols) and electron exchange capacities (EECs) (horizontal bars) during redox cycling of hazelnut (HZ), douglas fir (DF), rice straw (RS) and chestnut wood (CW) char specimen. Changes in the EECs during redox cycling are expressed relative to the EEC of the untreated chars (i.e., $EEC_i/EEC_{untreated}$ where *i* corresponds to the untreated, the borohydride (BH_4^-)-reduced and the O_2 re-oxidized char specimen). The $EEC_i/EEC_{untreated}$ values are shown both in numbers and as black dots on the left. The red line corresponds to $EEC_i/EEC_{untreated}$ of 1, and the outer lines correspond to ratios of 0.8 and 1.2 (i.e., deviations of 20% from the initial EECs). Changes in the relative redox states of the char specimen are expressed as the relative contributions of EAC and EDC values to the total EEC value of each sample (i.e., EAC/EEC and EDC/EEC).

Metal contents. The iron (Fe) and manganese (Mn) contents in the ash of grass and wood chars were quantified by microwave-assisted aqua regia and hydrofluoric acid digestion of the chars.[3] The elemental composition of the extracts was determined by an inductively coupled plasma optical emission spectrometer (Perkin Elmer Optima 3000DV). **Table S5** shows the total Fe and Mn concentrations in the char specimen and the ratios of Fe and Mn contents to the electron accepting capacities (EACs), electron donation capacities (EDCs) and electron exchange capacities (EECs) of the respective char specimen. The Fe and Mn contents of G700 and W700 char were not determined. The small Fe and Mn contents and the small ratios of these elements to

the EAC, EDC and EEC values, respectively, strongly suggest that these two metals only had minor contributions to the redox capacities determined for the thermosequence chars.

Table S5. Concentrations of manganese (Mn) and iron (Fe) in the thermosequence grass and wood chars expressed in absolute numbers and as ratios to the electron accepting capacities (EAC), electron donation capacities (EDC) and electron exchange capacities (EEC) of the chars.

	Metal contents [mmol (g char)$^{-1}$]		Metal to EAC ratio [mmol metal / mmol e-]		Metal to EDC ratio [mmol metal / mmol e-]		Metal to EEC ratio [mmol metal / mmol e-]	
	Mn	Fe	Mn	Fe	Mn	Fe	Mn	Fe
G700	-	-	-	-	-	-	-	-
G600	0.010	0.017	0.02	0.03	0.10	0.17	0.01	0.02
G500	0.009	0.004	0.01	0.01	0.03	0.02	0.01	0.00
G400	0.010	0.055	0.01	0.06	0.01	0.08	0.01	0.03
G300	0.010	0.040	0.17	0.72	0.03	0.12	0.02	0.10
G200	0.008	0.016	0.38	0.77	0.06	0.13	0.05	0.11
W700	-	-	-	-	-	-	-	-
W600	0.009	0.001	0.06	0.00	0.33	0.02	0.05	0.00
W500	0.014	0.001	0.02	0.00	0.43	0.02	0.02	0.00
W400	0.013	0.001	0.05	0.00	0.08	0.01	0.03	0.00
W300	0.010	0.004	0.65	0.24	0.05	0.02	0.05	0.02
W200	0.012	0.006	2.47	1.17	0.08	0.04	0.08	0.04

Accumulation of redox active moieties. Both the grass and the wood thermosequence chars show an increase in the EAC and EEC values with increasing HTT. There are two plausible explanations for the measured increases: either electron accepting moieties were newly formed during the charring process (and the neo-formation increased with increasing HTT) or electron accepting moieties present in the low-HTT chars (i.e., G200 and W200) accumulated relative to redox-inactive constituents during the charring process. To assess the latter possibility, we first estimated the maximum possible EAC and EEC values of chars formed at HTT> 200°C, EAC_{accum}(G/WX00) and EEC_{accum}(G/WX00) (both [mol e- $(g_{char})^{-1}$]), assuming that all electron accepting moieties for EAC and all redox-active moieties for EEC in the respective 200°C chars were preserved during charring:

$$\mathrm{EAC_{accum}(G/WXOO)} = \mathrm{EAC_{G/W200}} \cdot \frac{\mathrm{yield_{G/W200}}}{\mathrm{yield_{G/WX00}}} \qquad \textbf{Eq. S2a}$$

$$\mathrm{EEC_{accum}(G/WXOO)} = \mathrm{EEC_{G/W200}} \cdot \frac{\mathrm{yield_{G/W200}}}{\mathrm{yield_{G/WX00}}} \qquad \textbf{Eq. S2b}$$

where $EAC_{G/W200}$ and $EEC_{G/W200}$ (both [mmol e- $(g_{char})^{-1}$]) are the EAC and EEC values of the G/W200 chars, respectively, and $yield_{G/W200}$ and $yield_{G/WX00}$ (both [mass %]) are the charring yields for the G/W200 and the G/WX00 chars, respectively (**Table S6**, data from reference[1]).

We then related EAC_{accum}(G/WX00) and EEC_{accum}(G/WX00) to the experimentally measured $EAC_{G/WX00}$ and $EEC_{G/WX00}$ values (both [mmol e- $(g_{char})^{-1}$]):

$$\text{Max. contribution of accumulation to EAC } [\%] = \frac{EAC_{accum}(G/WX00)}{EAC_{GX00}} \cdot 100 \qquad \textbf{Eq. S3a}$$

$$\text{Max. contribution of accumulation to EEC } [\%] = \frac{EEC_{accum}(G/WX00)}{EEC_{GX00}} \cdot 100 \qquad \textbf{Eq. S3b}$$

The results of the calculations for all chars, including calculations for EDC values, are shown in **Table S6**. The data shows that an accumulation of electron accepting moieties in the G200 and W200 chars could explain at most 11% and 13% of the EAC values of the grass and wood chars formed at HTT≥ 400°C, respectively. This finding implies that electron accepting moieties had to be newly formed during charring at HTT≥ 400°C. Also, an accumulation of electron donating moieties in G200 and W200 would have resulted in a much larger than measured EDC values of the grass and wood chars formed at HTT≥ 400°C. Charring therefore resulted in a loss of electron donating moieties that were present in the low-HTT chars.

Table S6. Char yields after charring for 1h at the respective charring temperatures (data from reference[1]) and estimated maximum contribution of accumulated electron accepting or donating moieties of 200 °C chars to the measured EAC, EDC and EEC values.

Sample	Yield [mass %]	Maximum contribution of accumulation to measured redox capacities [% of measured values]		
		EAC	EDC	EEC
G700	28.8	9.1	375	57
G600	29.8	10.7	398	66
G500	31.4	7.7	159	43
G400	37.2	5.8	46	23
G300	75.8	46.5	46	46
G200	96.9	100.0	100	100
W700	22.0	9.8	2100	270
W600	23.9	13.2	2200	350
W500	28.4	3.1	1670	90
W400	35.3	5.2	200	90
W300	62.2	48.4	114	110
W200	95.9	100.0	100	100

Carbon oxidation state. The average oxidation state of carbon in the char specimen, C_{ox}, was calculated using **Equation 2** in the manuscript.[4] **Figure S5** shows the trends in C_{ox} values with HTT for the grass and wood thermosequence chars. For all chars, three C_{ox} values were calculated based on the assumptions that (i) the N contents of the chars were sufficiently small to not affect C_{ox} (i.e., [N] = 0), (ii) all N in the chars was present in the most positive (oxidized) oxidation state (i.e. k= +5) and (iii) all N in the chars was present in the most negative (reduced) oxidation state (i.e., k= -3). The N contents in all chars are very small (N <0.9 wt %) and chars from the same feedstock have very similar N contents, independent of the heat treatment temperature (**Table 1**). **Figure S5** shows that calculations based on the three assumptions resulted in comparable C_{ox} values, particularly for the wood chars. More importantly, the different assumptions did not affect the trends in the C_{ox} values with HTT.

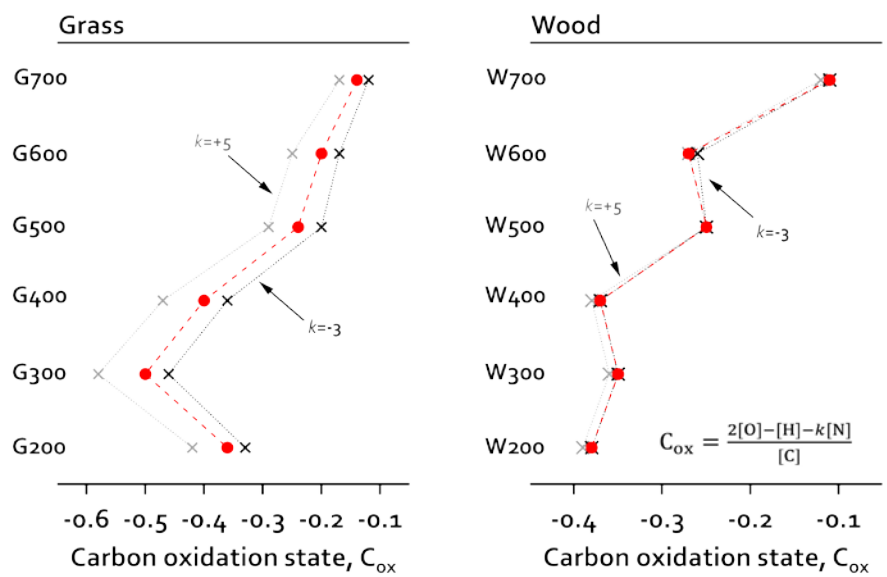

Figure S5. Calculated average oxidation states of carbon, C_{ox}, in the thermosequence grass (G; panel a) and wood (W; panel b) char specimen. The red data points were calculated assuming that nitrogen contents, [N], of the chars were sufficiently small to not affect C_{ox} (data also shown in **Figure 2c,d** in the manuscript). The grey and black data points and lines represent C_{ox} values calculated based on the assumption that all nitrogen in the chars were present either in their most oxidized form (i.e., k= +5) or in their most reduced form (i.e., k= -3), respectively. All three calculations resulted in comparable trends of C_{ox} with heat treatment temperature for the grass and the wood thermosequence chars.

Ratios of electron accepting and electron donating capacities to oxygen and carbon contents. We propose that the redox capacities of chars are associated with the organic (carbon) fraction of the thermosequence chars and that quinone and phenolic moieties largely contribute to the EAC and the EDC values, respectively. In a plausibility analysis, we assessed which percentage of the C and O atoms of the chars would need to be redox active to explain the measured EAC and EDC values. **Figure S6 a,b** shows that for both grass and wood chars the ratio of all EAC and EDC values to the total carbon content were below 1.5%, suggesting that only a very small fraction of the carbon had to be associated with redox-active moieties. The ratios of the EAC and the EDC values to the total oxygen contents were larger (**Figure S6 c,d**): we calculated that between 0.1% (G200) and 33% (G700) and between 0% (W200) and 6% (W500 and W700) of the oxygen atoms in the grass and wood chars, respectively, had to be electron accepting to explain the measured EAC values. For the EDC values, less than 7% (G400) and 1.5% (W400) of the oxygen atoms in the grass and wood chars had to be electron donating to explain the measured EDC values. This plausibility analysis shows that the chars contained sufficiently high oxygen contents to explain the EAC and EDC values with electron transfer to quinone moieties and from phenolic moieties, respectively. The relatively high EAC/[O] ratio of G700 suggests that non-oxygen containing electron accepting structures may have contributed to the measured EAC values of this high HTT material. We propose that polyaromatic, (sub-)structures are the most likely candidates as these accept electrons and require high HTT to be formed.

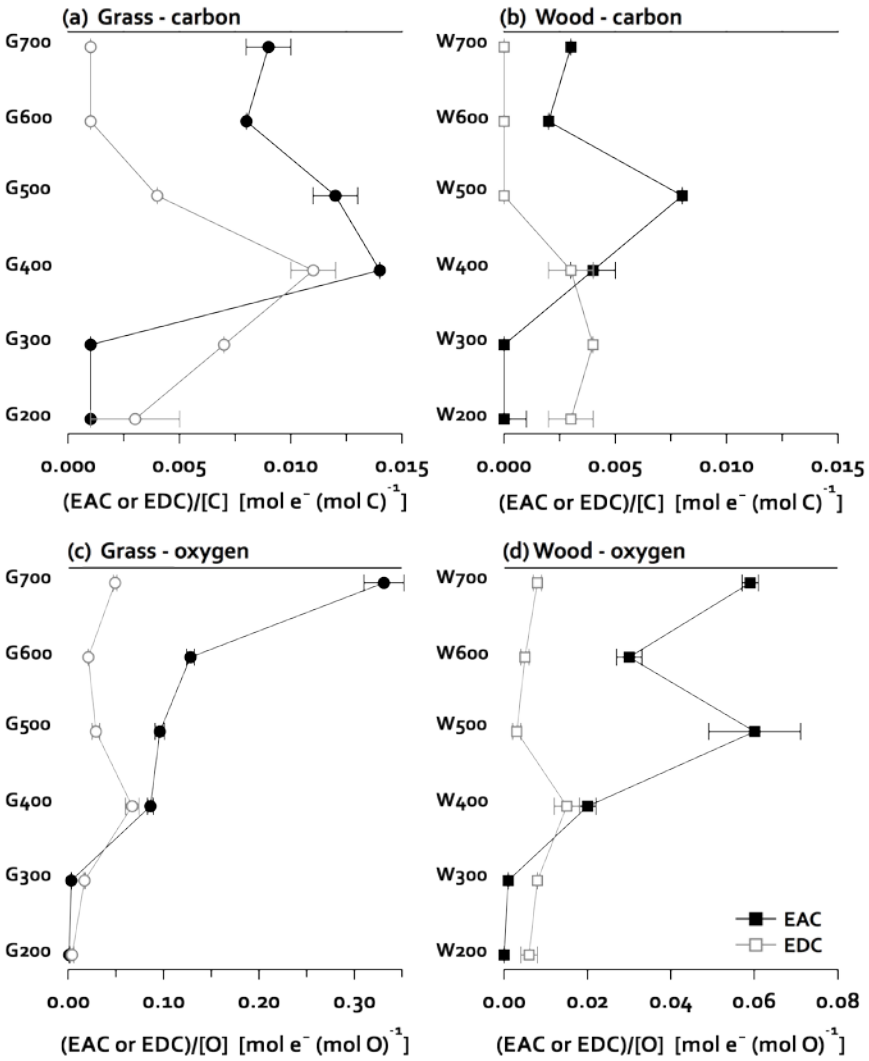

Figure S6 a,b. Ratios of the electron accepting capacities (EAC; black symbols) and electron donating capacities (EDC; grey symbols) of grass (panels a and c) and wood (panels b and d) thermosequence chars to their respective carbon contents (panels a,b) and oxygen contents (panels c,d).

Electron accepting and donating capacities of lignin, cellulose, and graphite. In addition to analyzing the different char specimen, we also quantified the EAC and EDC values of lignin (alkali, low sulfonate content, 471003 Aldrich), cellulose (from spruce, acid washed, 0.02-0.15mm fibers, 22182 FLUKA), and graphite (powder from graphite rods, 150mm long, Ø 6mm, 99.995%, high density, 496561 Aldrich). Lignin and cellulose were used as purchased; graphite

powder was obtained by scraping particles off the rods with a spatula. The three materials were suspended similar to the char samples in 0.1 M KCl, 0.1 M phosphate buffer at pH 7 (1 g L^{-1}). The reductive and oxidative current responses in MER and MEO of the three materials and the respective EAC and EDC values are given in **Figure S7**. The tested lignin had a high EDC of 4.32 mmol e^- (g lignin)$^{-1}$ and a comparatively small EAC of 0.25 mmol e^- (g lignin)$^{-1}$. The tested cellulose was redox inactive in both MER and MEO. The graphite had small EAC and EDC values of 0.03 and 0.01 mmol e^- (g graphite)$^{-1}$, respectively.

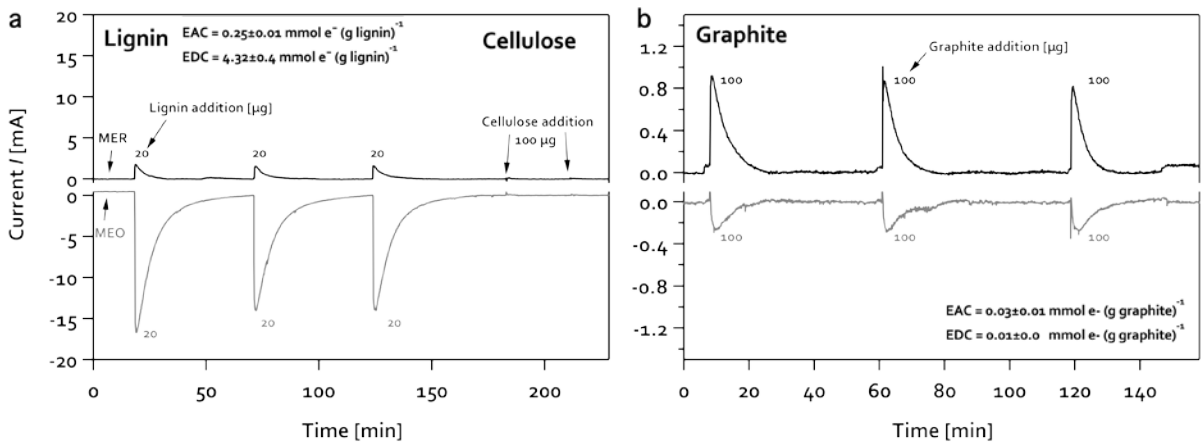

Figure S7. Current responses in mediated electrochemical reduction (MER, -0.49 V, pH 7; black traces) and oxidation (MEO, +0.61 V, pH 7; grey traces) of lignin and cellulose (both in panel a) and graphite (panel b) and the corresponding electron accepting and donating capacities (EAC and EDC). Errors represent standard deviations from triplicate measurements.

Estimation of quinoid C=O contents. The contents of quinoid C=O groups were estimated based on the C 1s NEXAFS spectra reported by Keiluweit et al. (2010).[1] The most characteristic feature of the quinoid structure is the red shift of the first ring C 1s-π* resonance towards 284 eV.[5] This shift is thought to be largely associated with a lower π^*_{LUMO} (lowest unoccupied molecular orbital) energy, and seen as a clear indication of a loss of aromatic stabilization due to quinoid distortion (up to -1.6 eV).[5] We note that a red shift towards 284 eV has also been observed for ring C 1s-π* resonances of condensed aromatic compounds and O-substituted aromatics, but these shifts are comparatively small (~ -0.1 to -0.3 eV).[6-9] We therefore interpret

the absorbance at 284 eV as being largely due to the presence of quinoid C=O groups in aromatic-like C structures. To quantify the relative absorbance at 284 eV, normalized NEXAFS spectra were de-convoluted with Gaussian peaks as described in Keiluweit et al. (2012)[10] using the PeakFit software (SeaSolve Software Inc., San Jose, CA, USA).

Based on the resulting peak areas, the quinoid C=O content, c(quinoid C=O) [mol C=O (g char)$^{-1}$], was calculated as follows:

$$c(quinoid\ \mathrm{C=O}) = \frac{peak\ area\ (quinoid\ C=O)\ (=resonance\ A)}{total\ peak\ areas\ (O-containing\ groups)\ (=\Sigma\ resonances\ A,C,D,F)} \times c(O)_{total}$$

where the "total peak area o-containing groups" is the sum of the peak areas for resonances of O-containing functional groups at the C K-edge (Resonances A, C, E, and F in **Table S7**) and $c(O)_{total}$ [mol O (g char)$^{-1}$] is the molar O content of the char.

Table S7. Peak areas for resonances of O-containing functional groups at the C K-edge used to normalize the quinone C=O peak area.

Peak position (eV)	Assignment	Transition	Resonance
284.4	Quinone C=O	1s-π*	A
285.3	Aromatic C=C	1s-π*	B
286.5	Aromatic C=C-O	1s-π*	C
287.5	Aliphatic C-H	1s–3p/σ*	D
288.5	Carboxylic C=O	1s-π*	E
289.5	Alcoholic C-O	1s–3p/σ*	F

The estimated quinoid C=O contents for each char are given in **Table S1**.

Comparison of electron accepting capacities to the quinoid C=O contents of the chars.

Figure S8 shows that the ratios of the EAC values to the quinoid C=O contents increased with increasing HTT from 0.2 and 0.1 mol e- (mol C=O)$^{-1}$ for G300 and for W300, respectively, to 0.94 and 0.19 mol e- (mol C=O)$^{-1}$ for the G700 and W500 thermosequence chars. The high ratio

of EAC to quinoid C=O contents of approximately unity for G700 suggests that most quinone groups had to be electroactive to explain the measured EAC values. Alternatively, the high ratio of EAC to quinoid contents may also signify that non-quinoid structures, such as conjugated Π–electron systems, contributed to the EAC at high HTT.

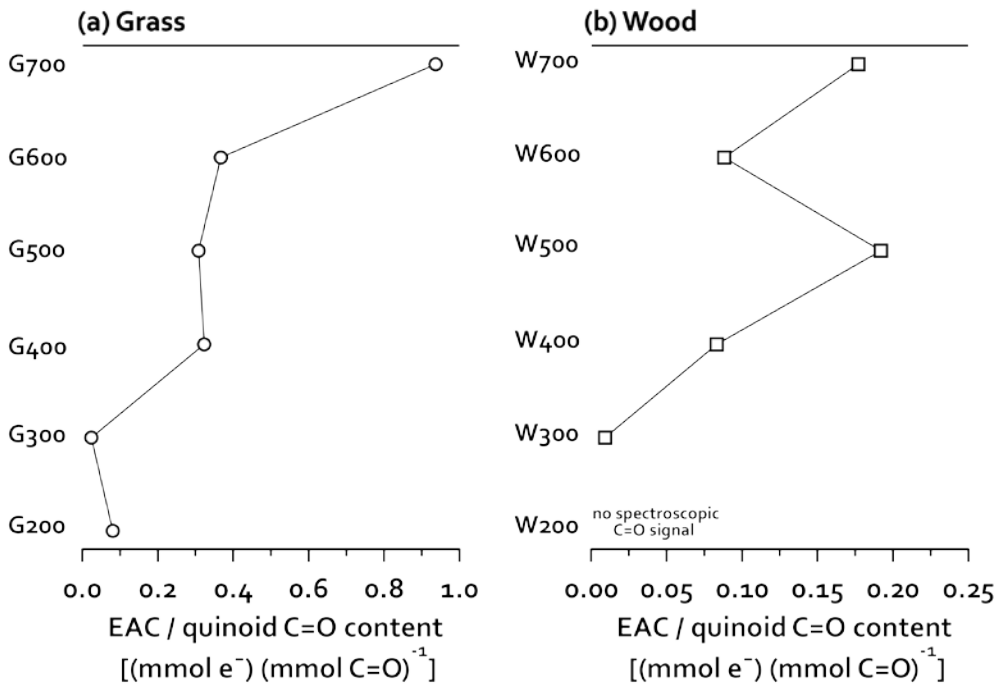

Figure S8. Ratios of the EAC values to the estimated quinoid C=O contents for the different specimen of the grass (G; panel a) and wood (W; panel b) char thermosequences.

Aromaticities of chars. We estimated the changes in the aromaticities of grass and wood thermosequence chars with increasing HTT by calculating the double bond equivalents (DBE; **equation S4**) and the aromaticity index (AI; **equation S5**) of the different char specimen according to reference [2]:

$$\mathrm{DBE}_{\mathrm{per\ C}} = \frac{\mathrm{DBE}}{[\mathrm{C}]} = \frac{1+[\mathrm{C}]-0.5\cdot[\mathrm{H}]+0.5\cdot[\mathrm{N}]}{[\mathrm{C}]} \qquad \textbf{Eq. S4}$$

$$\mathrm{AI} = \frac{\mathrm{DBE}_{\mathrm{AI}}}{\mathrm{C}_{\mathrm{AI}}} = \frac{1+[\mathrm{C}]-[\mathrm{O}]-0.5\cdot[\mathrm{H}]}{[\mathrm{C}]-[\mathrm{O}]-[\mathrm{N}]} \qquad \textbf{Eq. S5}$$

The DBE value is a measure of double bonds in a molecule[2] and, therefore, can be used as a proxy for the content of aromatic structures. Compared to the DBE value, the AI value is a more conservative estimate of aromaticity as it accounts for potential contributions of heteroatoms (i.e. O, N, S, P) to the overall double bond contents (i.e., the AI accounts for the fact that double bonds involving heteroatoms do not have to contribute to aromaticity, ring formation or condensation). The AI values can be used to assess whether molecules contain condensed aromatic structures: all molecules with AI$\geq$ 0.67 (which is the AI of benzene) must contain condensed ring systems. The value of AI= 0.67 is also referred to as the condensation threshold.

The DBE and AI values for the thermosequence grass and wood chars are shown in **Figure S9**. Negative AI values calculated for G200, G300, W200, and W300 were set to zero (per definition: if $DBE_{AI} \leq 0$ or $C_{AI} \leq 0$, then AI= 0). We note that an AI value ≤ 0 for a given material does not imply that this material does not contain aromatic structures (because AI provides a conservative estimate of the number of aromatic double bounds). For both thermosequences, chars formed at HTTs$\leq$ 400°C had smaller AI then DBE values. The differences between AI and DBE values in the low-HTT chars reflect their relatively high O contents in comparison to the chars formed at higher HTT (**Table S1**). The differences between the AI and DBE values for the chars formed at HTTs$\geq$ 500°C were much smaller, reflecting the fact that the O contents (and hence their potential contributions to double bonds) largely decreased with increasing HTT (**Table S1**). Both grass and wood chars exceed the condensation threshold (AI= 0.67) for HTT$\geq$ 500 °C, consistent with spectroscopic data, which provided evidence for increasing ring condensation at HTT $\geq$ 500 °C.[1]

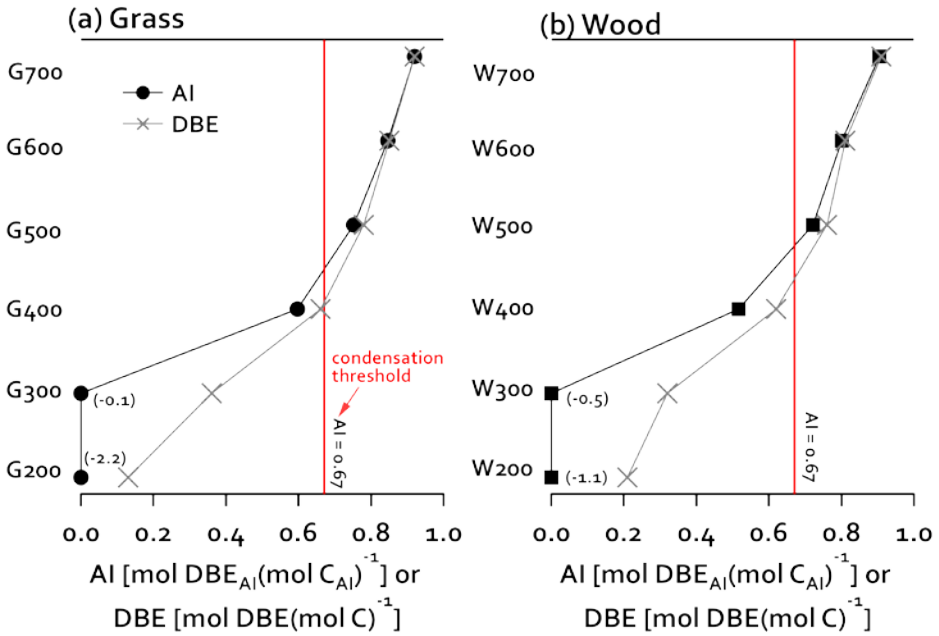

Figure S9. Changes in double bond equivalents (DBE; grey symbols) and aromaticity index values (AI; black symbols) of grass (G; panel a) and wood (W; panel b) thermosequence chars. Negative AI values for G200, G300, W200, and W300 were, per definition, set to zero (calculated values for these chars are shown next to the respective data points). The red line at AI = 0.67 corresponds to the condensation threshold above which a molecule must contain condensed aromatic rings (i.e., benzene has an AI= 0.67).

References

1. Keiluweit, M.; Nico, P. S.; Johnson, M. G.; Kleber, M.; Dynamic molecular structure of plant biomass-derived black carbon (biochar). *Environmental Science & Technology* **2010,** *44*, (4), 1247-1253.
2. Koch, B. P.; Dittmar, T.; From mass to structure: an aromaticity index for high-resolution mass data of natural organic matter. *Rapid Commun. Mass Spectrom.* **2006,** *20*, (5), 926-932.
3. Hossner, L. R., Dissolution for Total Elemental Analysis. In *Methods of Soil Analysis Part 3—Chemical Methods*, Sparks, D. L.; Page, A. L.; Helmke, P. A.; Loeppert, R. H., Eds. Soil Science Society of America, Inc., American Society of Agronomy, Inc.: Madison, WI 1996; pp p. 49-64.
4. Masiello, C. A.; Gallagher, M. E.; Randerson, J. T.; Deco, R. M.; Chadwick, O. A.; Evaluating two experimental approaches for measuring ecosystem carbon oxidation state and oxidative ratio. *Journal of Geophysical Research* **2008,** *113*, (G3), G03010.
5. Francis, J. T.; Hitchcock, A. P.; Inner-shell spectroscopy of para-benzoquinone, hydroquinone, and phenol - distinguishing quinoid and benzoid structures. *Journal of Physical Chemistry* **1992,** *96*, (16), 6598-6610.

6. Baldea, I.; Schimmelpfennig, B.; Plaschke, M.; Rothe, J.; Schirmer, J.; Trofimov, A. B.; Fanghanel, T.; C 1s near edge X-ray absorption fine structure (NEXAFS) of substituted benzoic acids - A theoretical and experimental study. *Journal of Electron Spectroscopy and Related Phenomena* **2007,** *154*, (3), 109-118.

7. Agren, H.; Vahtras, O.; Carravetta, V.; Near-edge core photoabsorption in polyacenes - model molecules for graphite. *Chemical Physics* **1995,** *196*, (1-2), 47-58.

8. Solomon, D.; Lehmann, J.; Kinyangi, J.; Liang, B. Q.; Heymann, K.; Dathe, L.; Hanley, K.; Wirick, S.; Jacobsen, C.; Carbon (1s) NEXAFS Spectroscopy of Biogeochemically Relevant Reference Organic Compounds. *Soil Science Society of America Journal* **2009,** *73*, (6), 1817-1830.

9. Kuznetsova, A.; Popova, I.; Yates, J. T.; Bronikowski, M. J.; Huffman, C. B.; Liu, J.; Smalley, R. E.; Hwu, H. H.; Chen, J. G. G.; Oxygen-containing functional groups on single-wall carbon nanotubes: NEXAFS and vibrational spectroscopic studies. *Journal of the American Chemical Society* **2001,** *123*, (43), 10699-10704.

10. Keiluweit, M.; Bougoure, J. J.; Zeglin, L. H.; Myrold, D. D.; Weber, P. K.; Pett-Ridge, J.; Kleber, M.; Nico, P. S.; Nano-scale investigation of the association of microbial nitrogen residues with iron (hydr)oxides in a forest soil O-horizon. *Geochimica Et Cosmochimica Acta* **2012,** *95*, 213-226.